

What can the highest angular resolution bring to stellar astrophysics?
F. Millour, A. Chiavassa, L. Bigot, O. Chesneau, A. Meilland and Ph. Stee (eds)
EAS Publications Series, Vol. 69-70, 2014, p.319

STAR FORMATION AT MILLI-ARCSECOND RESOLUTION

René D. Oudmaijer¹ and Willem-Jan de Wit²

Abstract. This chapter discusses the use and possibilities of optical and infrared interferometry to study star formation. The chapter starts with a brief overview of the star formation process and highlights the open questions from an observational point of view. These are found at the smallest scales, as this is, inevitably, where all the action such as accretion and outflows, occurs. We then use basic astrophysical concepts to assess which scales and conditions can be probed with existing interferometric set-ups for which we use the ESO/VLTI instrument suite as example. We will concentrate on the more massive stars observed at high resolution with continuum interferometry. Throughout, some of the most recent interferometric results are used as examples of the various processes discussed.

1 Introduction

The basic principle of the gravitational collapse of a molecular cloud leading to the formation of a young star has been known since the ground-breaking work by Jeans in the early 20th century. Indeed, Jeans' major insight has led to significant progress in our understanding of the star formation process. The prevailing formation scenario for low mass stars, was outlined in detail in their standard work by Shu et al. 1994. In short, after the dense, cold molecular cloud collapses, conservation of angular momentum implies that the system rapidly spins up, leading to the formation of a circumstellar disk around the central star. Matter will continue to accrete onto the star through this accretion disk, while bi-polar jets emanate from the polar regions of the newly formed star. The disk not only feeds the star, but also acts as birth place of possible planets. This paradigm of collapsing clouds forming stars has been observationally verified and forms the basis of our understanding of low mass star formation.

For more massive stars, progress has been slower, both theoretically and observationally. A key difference is that the lower mass, Sun-like, stars sustain magnetic

¹ School of Physics & Astronomy, University of Leeds, Woodhouse Lane, Leeds LS2 9JT, UK

² European Southern Observatory, Casilla 19001, Santiago 19, Chile

fields, and grow via magnetically controlled accretion through a disk. In contrast, higher mass stars have radiative envelopes and are not magnetic. They are thus not necessarily expected to form in a similar manner to low mass stars. In addition, the larger masses and therefore larger stellar luminosities involved pose their own difficulties as the stars' enormous power output results in a strong radiation pressure which may halt the accreting material altogether and prevent the stars to grow to very high masses. Recently Krumholz et al. (2009) were able to show from high resolution computations that massive stars can indeed form by disk accretion. The radiation driven outflows are channeled through the bipolar cavity and consequently the disk undergoes less radiation pressure. Confirmation of this formation scenario revolves around the properties of the circumstellar material close to the star. Inevitably, this requires observations at the highest spatial resolution.

Observationally, the study of massive young stars is hampered by the fact that they are much rarer than lower mass stars, and therefore on average further away, requiring high resolution studies to probe the accretion region. This is one of the reasons that direct imaging of these objects was not possible for a long time. As an alternative, astronomers resorted to the next best diagnostic for studying the circumstellar material instead, the Spectral Energy Distribution (SED). The trouble however is that model fits of SEDs are not unique. They can be readily explained by both disks or spherical envelopes, and as a result very different star formation scenarios can be invoked based on the same data. The ambiguity associated with indirect methods is well illustrated by the lively debate in the nineties about the nature of the circumstellar material around the intermediate mass pre-Main Sequence Herbig Ae/Be stars. The debate concerned whether Herbig Ae/Be stars were surrounded by disks or not (see e.g. Waters & Waelkens (1998) for an overview at that time). Headway was only made when Mannings & Sargent (1997) detected rotating disk-like structures around Herbig Ae/Be stars, and the presence of disks was seemingly established. Not much later, Miroshnichenko et al. (1999) showed that the simultaneous presence of both disk and envelope can also explain the SED; the inner, warm, disk contributes to the near-infrared (NIR) excess, while a cooler spherical envelope dominates the longer wavelength excess emission. The case of disk accretion for Herbig Ae/Be was not yet settled however, as the large (200-600 au) disk-like structures observed at mm wavelengths are too far from the star to probe accretion.

It is important to note here that on several occasions flattened structures have been observed towards massive young stars, and these were often identified with disk accretion scenarios. However, this is a misconception, many such disk tracers only probed regions far out and thus can not at all be used to study the accretion process. This issue is often overlooked.

Not surprisingly, progress often goes hand in hand with technological advances, and star formation is not an exception. In particular the advent of milli-arcsecond resolution observations offers the prospects to study the inner regions where the accretion occurs.

1.1 *Properties of the circumstellar material*

Before we start discussing observations, and their interpretation, that have been performed at the highest resolution, it may be appropriate to first discuss a model of the geometry that we expect around these stars. In order to do so, we will first introduce some terminology and explain the various types of star in the framework of the classical Lada classification of the various stages of the formation of a star (Lada, 1987). In short, the class I sources are very cool: not much, if any, heating of the molecular cloud occurs and these objects are only visible at infrared and longer wavelengths. At a later stage, the class II sources show a flat spectrum, light from the accretion disk and the envelope dominate the SED, at near-infrared wavelengths and longer. The class III sources have dispersed these envelopes in their entirety and the SED is dominated by the star and disk. The Class II and III sources, being bright at near- and mid-infrared wavelengths ($K - N$ band), have their peak energy output in the ESO/VLTI wavelength range, while the Class I sources can be studied at the L , M and N bands. Hence the ESO/VLTI operating wavebands are particularly well matched to the young stars (or vice versa).

The types of low mass sources ($M < 2\text{-}3 M_{\odot}$) that we can study are the pre-main sequence T Tauri objects which are type II/III sources. Their counterparts at intermediate mass ($2\text{-}3 M_{\odot} < M < 10\text{-}15 M_{\odot}$) are the pre-main sequence Herbig Ae/Be stars. At higher masses there is no obvious, observable, pre-Main Sequence phase, as the stars evolve much faster and arrive on the Main Sequence while still embedded in their envelopes. In a way, the objects under consideration, the Massive Young Stellar Objects (MYSO) can be compared to the class I objects.

A picture of their circumstellar environment is provided in Fig. 1. The star is embedded in a dense envelope, surrounded by an accretion disk, while the radiation pressure from the star drives a flow which carves a bipolar cavity in the envelope.

1.2 *Observations of the circumstellar material*

Many breakthroughs in this field over the last years have been made with the new generation optical/infrared interferometric instrumentation. These made observations of the inner disks and the bases of the outflows at milli-arcsecond scales possible. This is at scales which are orders of magnitude smaller than the outer disks detected and probed by infrared and (sub-)mm observations obtained thus far. The inner disks were first observed using single baselines which allowed basic size measurements. It was found that the inner boundaries of the disks get larger as a function of luminosity, consistent with the notion that the dust sublimation radius is measured (as documented by e.g. Millan-Gabet et al. 2007, and discussed later). However, not all Herbig Ae/Be stars follow this relationship, and some objects turned out to be smaller than predicted. This has led to several suggestions for the nature of the near-infrared emission. Competing ideas include that the near-infrared emission comes from optically thick gas (Kraus et al. 2008), or that it is due to refractory grains which can survive higher temperatures (Benisty et al. 2010). Full model-independent images of several Her-

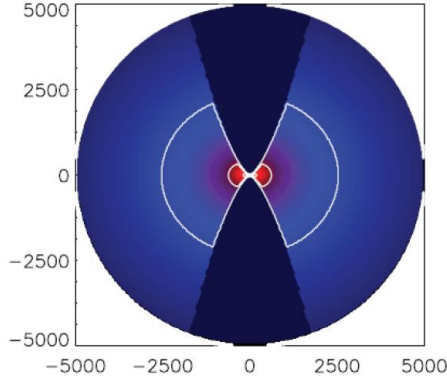


Fig. 1. A model representation of the circumstellar matter of a Massive Young Stellar Object. The central star is embedded in a dense dusty environment. The bi-polar flow has carved a cavity, while the equatorial condensation may signpost a dense accretion disk. The scales are in au. From Whitney et al. (2003)

big Ae/Be stars have now been published, proving beyond doubt that the objects are surrounded by disks (e.g. Benisty et al. (2011) and references therein). In parallel, the next step is to fully understand and parametrize the properties of the disks in order to follow the formation and evolution of intermediate and massive stars. An early example has been published by Weigelt et al. (2011) who took advantage of the high spectral resolving power of VLTI/AMBER ($R \sim 12000$) and both spectrally and spatially resolved the $\text{Br}\gamma$ line of the Herbig Be star MWC 297 which has a spectral type of B1.5Ve. By fitting the spectral line, they suggest that the emission is due to a disk-wind.

Finally, there are the more embedded Massive Young Stellar Objects with masses exceeding $10\text{--}15 M_{\odot}$, these are on average even further away than Herbig Ae/Be stars, with as added complication that they are optically invisible due to the large extinction. Using AMBER data at $2\mu\text{m}$, Kraus et al. (2010) present tantalizing evidence for disks around these most massive young stars as well.

In this chapter we will first discuss what we can probe at the smallest scales for young stars. We then discuss the power and limitations of optical/infrared (OIR) interferometric data in understanding the properties of these objects. We continue describing the efforts in interpreting the data supported by radiative transfer models and highlight the various pitfalls. We conclude the chapter with a number of exercises. We will not be able to discuss every aspect of star formation, and will focus here on the more massive stars and high resolution OIR continuum interferometry. A very recent overview of the field can be found in the review papers of the Protostars and Planet VI conference held in Heidelberg in 2013 (www.ppvi.org). This chapter also touches upon many topics discussed in this

book, of which the contributions by Bonneau et al. (binary stars), and Meilland & Stee (disk diagnostics) are of note.

2 What we are probing at small scales

At the wavelengths the VLTI operates (AMBER: H, K , MATISSE: L, M , MIDI: N , hence $1.6 \mu\text{m}$ to $10 \mu\text{m}$), the observed flux from young stars is dominated by thermal emission from dusty particles, whose temperature determines the peak wavelength. The dust temperature is a function of distance to the star which we can relate to angular size scales using some basic astrophysical principles.

Assuming that a dust grain acts like a black body, and re-radiates all the energy it absorbs, it can be shown that the temperature of a dust grain depends only on its distance from the star and the star's luminosity. Using Wien's displacement law ($\lambda T \approx 3 \times 10^{-3} \text{ mK}$), we can determine at which wavelengths the dust radiation dominates, and therefore relate astrophysical size scales to the observational set-ups required. We leave the specifics of the derivation of the relationships between the dust temperature, T_d , the stellar parameters (temperature and radius, T_*, R_*), and the distance of the dust to the star, d as an exercise to the reader at the end of this chapter. The result can be written as:

$$T_d = \sqrt{\frac{R_*}{2d}} T_* \quad (2.1)$$

Intuitively, this equation makes sense, the higher the star's temperature and radius, the more energy it emits and hence more energy is absorbed by a dust particle. In contrast, the larger the distance between star and dust, less energy is absorbed. Given that $L_* \propto R_*^2 T_*^4$, we can see that $T_d^2 \propto \sqrt{L_*}/d$. The radius of the dust grains cancel out in the derivation. This is because the energy absorbed by the grain and that radiated away by it are both dependent on the dust grain radius squared.

Knowing the dust temperature, we can then obtain an estimate of the distances probed at the various emitted wavelengths. An interesting early result demonstrating this relationship was obtained by Millan-Gabet et al. (2007). Using single-baseline optical interferometry, they measured the angular sizes of the dust emitting regions of a sample of young stellar objects at the K band. This wavelength probes, to first order, the inner parts of the disks at the dust sublimation temperature, the highest possible temperature below which dust can exist. The relationship above then reduces to $d \propto \sqrt{L_*}$, which is precisely what these authors observed for a sample of objects. Remarkably, the luminosities of their objects spanned five orders of magnitude. Recently, it has been found that Active Galactic Nuclei follow this relationship too (Kishimoto et al. 2011), extending the observed trend to galactic scales.

Let us now get a feel for the physical scales involved by evaluating Eq. 2.1 for a real Massive Young Stellar Object. Assuming the central star can be approximated by a Main Sequence star, a typical MYSO has $R_* = 8.4 R_\odot$ and temperature 35000

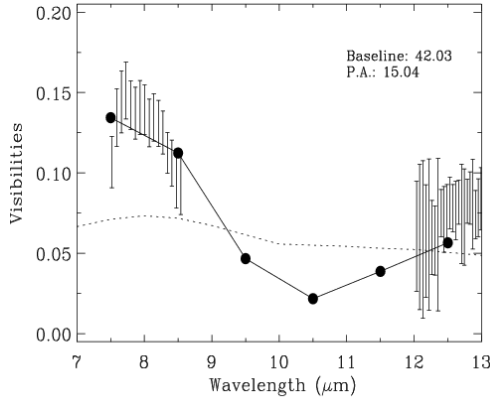


Fig. 2. The visibility of the Massive Young Stellar Object W33A from 8-13 μm as seen by MIDI on one baseline. The visibilities decrease with increasing wavelength, while the central silicate absorption at 10 μm is so deep, that no flux nor visibilities could be reliably measured. The lines denote various model fits to the data. Figure taken from de Wit et al. (2010).

K (e.g. W33A in de Wit et al. 2007). For a typically high dust temperature of 1000 K, we get

$$d = \left(\frac{T_*}{T_d} \right)^2 \left(\frac{R_*}{2} \right) = 24 \text{ au}$$

At a distance of 3.8 kpc, this corresponds to 6 milli-arcseconds, angular scales for which VLTI/AMBER is excellently suited and the success of the application of the VLTI, and other arrays, to Herbig Ae/Be stars is testament to this. However, with the exception of precious few published stars, many of these objects are too faint to be observed at the shorter wavelengths. The situation is even worse for the more embedded MYSOs. They are much brighter at longer wavelengths and can often only be observed at the MIDI N band.

However, observing at longer wavelengths introduces a complication, because the spatial resolution becomes worse at longer wavelengths as the resolution, R is proportional to $\frac{\lambda}{2B}$. Therefore, one could argue that MYSOs would become progressively less resolved at these longer wavelengths. However an interesting property of these objects is that they become larger with increasing wavelength, as these longer wavelengths trace cooler material. Using Wien's law, we find the MIDI wavelength range is sensitive to warm dust at 300 K. As shown above when we considered the dust which absorbs radiation and re-emits it as a black body, the distance increases with the inverse of the temperature squared, and this dust is located ~ 60 mas from the star. So, the saving grace in this situation is that the object is actually more resolved for the same set-up and baseline B at longer

wavelengths. The distance from the star increases with λ^2 (as λT is constant), and the “resolvedness” (for want of a better term) of these objects increases with λ . An illustration of this effect is provided in Figure 2. The figure shows the visibilities of a MIDI spectrum of a MYSO (W33A, data taken from de Wit et al. 2010). The spectrum covers the wavelength range from 8 to 13 μm . The 10 μm silicate absorption feature is so strong that no correlated flux could be measured in this line, but it is clear that the visibilities decrease as a function of wavelength, as predicted.

3 Interpreting the interferometric data

The discussion above illustrates both the power of high spatial resolution interferometry, but also its limitations. The single baseline visibilities allow for the determination of size scales and multiple baselines, or even model independent images, enable us to determine the geometry of the dusty material. However, astrophysical properties can not be derived from geometric information alone. For example, the analysis of the largest published MIDI dataset of MYSOs by Boley et al. (2013) is necessarily rudimentary and the authors can not conclude from their data and geometric analysis which particular structure is responsible for the N -band emission. Indeed, in-depth studies of individual objects using computer (and labour) intensive interpretation are needed to make progress. It is the combination of observations of large samples underpinned by in depth studies that allow progress to be made.

3.1 Modelling the Spectral Energy Distribution

One of the main aims in YSO research is to determine the parameters of the circumstellar material, the dust mass, its distribution and geometry.

A very powerful instrument in the astronomer’s toolbox is the modelling of the spectral energy distribution (SED) of an object. The method is fully based on the principles outlined earlier. The distance of a dust grain to the star and the star’s properties determine the temperature of the dusty particle which emits as a black body. The larger the particles, more flux will be absorbed and re-radiated, so the particle size, or even size distribution, determines the total outgoing infrared flux. The emergent radiation from a source embedded in a dust cloud is then the sum of the radiation of all dust particles that we can see. The challenge is to find which combination of star and dust particles can reproduce the SED.

Sometimes the infrared emission has the same shape as the Planck function, implying that effectively the dominant dust emission can be reproduced by a thin shell where all dust particles have the same temperature. If the infrared spectrum is flatter (or steeper), a different grain density as a function of distance from the star can be invoked. In the case of, for example, constant mass loss or accretion, the density follows a powerlaw $\rho(r) \propto r^{-2}$.

There are many models available that allow one to compute the SED from a star embedded in a dusty environment (e.g. Rowan-Robinson 1980, Whitney et al. 2003;

see also Ivezić et al. 1997). The basics of these models are similar, and the main differences are the levels of detail such as those of the stellar parameters (e.g. black body vs. stellar model), dust parameters (e.g. size distribution vs. single size, dust composition which affects the absorption and emission properties) and the implementation of the geometry (see later). Naturally, each refinement comes at the price of more input parameters. Some of these can be reliably set based on other information if available. These include for example the spectral type of the star when a stellar model is used as input, or the dust composition from an infrared spectrum, while others are free parameters that can only be determined through fitting. Depending on the complexity of the underlying model, many models can be computed fairly quickly on standard laptops and desktops.

In order to determine the input parameters of a dust model (and ultimately the properties of the dusty envelope) that provides the best fit to the SED one can use a formal fitting procedure, where the minimum χ^2 value is found by searching the entire parameter space. When the number of free parameters is large, an inordinate amount of computing time would be required to sample all possible combinations. In practice, minimum search algorithms such as AMOEBA are employed to reduce the computations required by specifically zooming in on the regions where the minimum χ^2 is located. An alternative is to compute a huge grid of models, and choose the best fitting one to the observed SED. An advantage is that this necessitates only one (long) run and multiple SEDs can be fitted in a short amount of time, whereas a disadvantage is that the grid does not necessarily cover all possible combinations of parameters. A good example is provided by Robitaille et al. (2007) who published a large grid of model SEDs, and posted the models and a bespoke fitting routine on the internet.

With the caveat that the number of free fit parameters can be large, it is in practice almost always possible to derive the number of particles, their density distribution and thus mass of the dusty envelope, from fitting the SED alone.

So far, we have not discussed the geometry of the material in terms of modelling the SED. Indeed, in many cases, spherical symmetry is assumed from the outset (e.g. in the case of evolved stars). As explained in the introduction, the SED modelling by itself can not discriminate between various spatial distributions of the dust. The infrared emission is not sensitive to the geometric location of the dusty particles. For example a spherical envelope or a disk geometry with identical density distributions will - with some dependence on the optical depth - both have the same temperature distribution and thus spectrum. It is thus hard to disentangle the geometry from the observed SED, i.e. the SED fitting is degenerate, and to break this degeneracy we need additional information.

To conclude, the high spatial resolution observations provide the geometry of the circumstellar material, but do not provide information on its astrophysical properties. The SED fitting can provide that information, but fails in determining the geometry. It may be clear that combining the two is the way forward in characterizing the material around MYSOs.

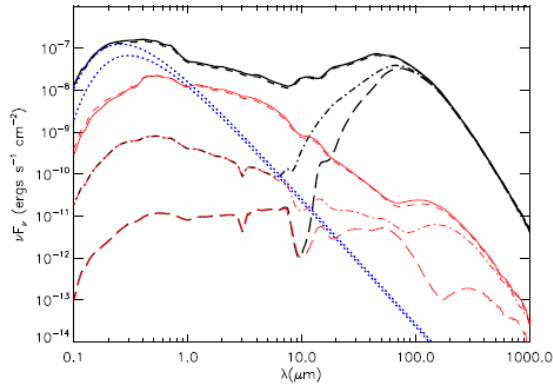


Fig. 3. The Spectral Energy Distribution for an MYSO model seen at various inclination angles. The dotted lines denote the stellar input models, while the observable SED is shown for different inclination angles. The thicker lines represent the total flux, the thin red lines represent scattered light. The top model is the face-on situation where we look inside the cavity, while the bottom model shows the edge-on case. The face-on model is brighter in general and shows more near-infrared emission, probing the inner regions, which are obscured from view in more edge-on situations. The edge-on models display much stronger silicate absorptions at $10\mu\text{m}$ for the same reason. Figure taken from Zhang & Tan (2011).

3.2 Two-dimensional models

Above we outlined the need for spatially resolved observations to break the degeneracy in SED modelling. This poses a number of challenges, some of them obvious, and some of them are perhaps less expected.

Firstly, the number of possible geometries that one can choose to model is unlimited, indeed, it would be limited only by our imagination. However, some geometries are more likely than others and this “free parameter” will have to be chosen *a priori*. In the case of Massive Young Stellar Objects, the paradigm of a spherically symmetric envelope with cavities carved out by a bi-polar flow, and a central star surrounded by a dense circumstellar disk is fairly well established (see also Figure 1). A widely used dust code which incorporates these elements is that by Whitney et al. (2003), while a more recent example is that of Zhang & Tan (2011). These codes allow the user to specify many geometrical parameters, some of which can be derived from other observations. The opening angle of the cavity can be found from larger scale scattered light observations in the K band (de Wit et al. 2010), while the inclination of the system can be inferred from other observations, such as for example CO rotational emission line imaging at mm wavelengths. Figure 3 demonstrates some of the dependencies involved.

It shows the emergent SED for the same dust model, which is seen at different inclinations. The resulting SEDs are markedly different, most notably, much more absorption occurs in the line of sight for the edge-on model, while the hot inner parts traced by the near-infrared emission are revealed in the face-on model.

Secondly, at the moment it is expensive to compute for a given geometry both the emergent SED and also the resulting image. It is therefore not feasible to probe the entire (free-)parameter space in the same manner as described above for the SED fitting, and choices have to be made to make the fitting process computationally more economical.

Thirdly, and perhaps surprisingly, it is not trivial to arrive at formal best fits when combining the spectral energy distribution and spatial information. Consider for example that a typical, well sampled, SED has of order 10-15 photometric points covering the range from the optical and near-infrared to millimetre wavelengths. A simple, single baseline visibility spectrum covering 8-13 μm such as shown in Fig. 2 already has more independent datapoints, and a formal reduced χ^2 would put less weight, if at all, to the SED, despite the fact that it probes a much larger temperature range than the MIDI spectrum.

We probably should point out at this stage that not many papers have had the luxury to combine excellent SED information with high spatial resolution data to constrain the circumstellar environments of MYSOs. The practice thus far is well summarized and explained in de Wit et al. (2010, 2011). In these papers, the authors first fix as many input parameters as possible by using all available information on the sources such as the stellar parameters and system inclinations. They also determine the cavity opening angle by using existing images in the near-infrared which probe the light scattered off the inner cavity walls. They then first consider the best fitting SED models from the grid computed by Robitaille et al. (2007). This limits the number of models that require the computation of model images. It should be noted here however, that many models fitting the SED do not match the spatial information. This is presumably due to the limited parameter space probed, but this approach does help narrowing down the possibilities. These authors then put equal weight to the information provided by the SED and the MIDI interferometric data respectively and looked for various models that simultaneously fit the SED and visibilities. A final check on the best fitting models was then done by comparing the model output at longer, mm, wavelengths with spatially resolved data. An example best fitting model is shown in Fig. 4 for the object AFGL 2136. The surprising finding in this case is the discovery of an unresolved central source that is strongly emitting in the mid-IR wavelength regime. This is hypothesized to be either a small, dense accretion disk or a bloated star whose extended atmosphere is the result of strong accretion onto the star.

4 Final Remarks

Remarkable progress has been made in star formation and the study of Massive Young Stellar Objects over the past decade. This is in no small part due to the

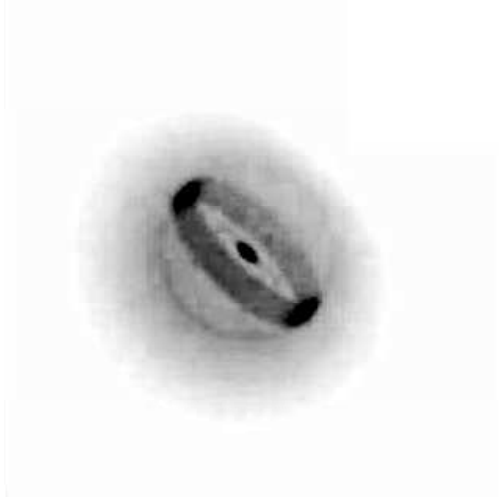


Fig. 4. An image at $10\mu\text{m}$ of a model which both fits the SED and interferometry for the MYSO AFGL 2136. The source consists of a bright, unresolved, structure in the center, which is surrounded by a dusty torus that is oriented in the NW-SE direction. The bi-polar flow shows a blue-shifted component in the South-Eastern direction and a red-shifted component to the North-West. The red-shifted component will be more obscured, as can also be seen in this figure, where the northern component is not visible. Shown is AFGL 2136 as per de Wit et al. (2011).

interferometric facilities having become mainstream and the observations themselves routine. So far however, the number of interferometrically observed objects is still limited, while the number of objects for which model independent images are available is even smaller.

The future holds much promise, the continually improving sensitivities will allow us to observe significantly more objects. In addition, instruments that can combine more baselines such as those on VLTI (PIONIER, MATISSE, combining 4 beams), CHARA (up to 6 beams), and MROI (10 elements), are either just installed on the telescope, or in an advanced stage of development and construction. This will make it much easier to obtain images and pave the way for statistical studies as it will be possible to begin studying the MYSOs observed in this manner

as function of their properties such as evolutionary state and mass.

The improved sensitivities will also allow us to move away from continuum work alone and enable studies of the emission lines. This will provide valuable information on the stellar parameters, accretion flow and bi-polar jets (e.g. Davies et al. 2010). Last but not least, the synergy with ALMA, which can achieve similar resolution, but probes cooler material, allows us to “map” the circumstellar environment of MYSOs from very close to the star to larger scales at unprecedented detail.

Exercises

1. Infrared emission is due to dust heated by the star’s radiation. The further dust is from the star, the cooler it is. Relate the distance d of a dust grain to a star as a function of the star’s radius R_* , temperature T_* and the dust grain’s temperature T_d . For this derivation, you can assume that the star radiates like a black body, and that a spherical dust particle absorbs 100% of the energy that falls on it, which it then re-radiates as a black body.
2. A typical Massive Young Stellar object has $T_* = 35000\text{K}$ and $R_* = 8.4$ solar radii, and is at a distance of 3.8 kpc. Now, take the dust grain at its sublimation temperature, say 1000K, and work out the angular distance of this dust grain to the star.
3. Most such objects are too faint for AMBER. With the help of Wien’s displacement law estimate which size scales and temperatures we can probe with MIDI.
4. We can now also check why T Tauri stars are rarely resolved with OIR interferometry. Look up the stellar parameters and distance typical for a T Tauri star and evaluate the size of the inner dust disk.

References

- Boley, P. A., Linz, H., van Boekel, R., Henning, T., Feldt, M., Kaper, L., Leinert, C., Müller, A., Pascucci, I., Robberto, M., Stecklum, B., Waters, L. B. F. M., Zinnecker, H. 2013, A&A 558, A24
- Benisty, M., Natta, A., Isella, A., Berger, J.-P., Massi, F., Le Bouquin, J.-B., Mérand, A., Duvert, G., Kraus, S., Malbet, F., Olofsson, J., Robbe-Dubois, S., Testi, L., Vannier, M., & Weigelt, G. 2010, A&A, 511, A74
- Benisty, M., Renard, S., Natta, A., Berger, J. P., Massi, F., Malbet, F., Garcia, P. J. V., Isella, A., Mérand, A., Monin, J. L., Testi, L., Thiébaud, E., Vannier, M., & Weigelt, G. 2011, A&A, 531, A84
- Davies, B., Lumsden, S. L., Hoare, M. G., Oudmaijer, R. D., de Wit, W.-J. 2010, MNRAS 402, 1504
- de Wit, W. J., Hoare, M. G., Oudmaijer, R. D., Mottram, J. C., 2007, ApJ 671, L169

- de Wit, W. J., Oudmaijer, R. D., Fujiyoshi, T., Hoare, M. G., Honda, M., Kataza, H., Miyata, T., Okamoto, Y. K., Onaka, T., Sako, S., & Yamashita, T. 2008, *ApJ*, 685, L75
- de Wit, W. J., Hoare, M. G., Oudmaijer, R. D., Lumsden, S. L., 2010, *A&A* 515, A45
- de Wit, W. J., Hoare, M. G., Oudmaijer, R. D., Nürnberger, D. E. A., Wheelwright, H. E., & Lumsden, S. L. 2011, *A&A*, 526, L5
- Ivezić, Z., Groenewegen, M. A. T., Men'shchikov, A., Szczerba, R. 1997, *MNRAS* 291, 121
- Kishimoto, M., Hönig, S. F., Antonucci, R., Barvainis, R., Kotani, T., Tristram, K. R. W., Weigelt, G., Levin, K., *A&A* 527, 121
- Kraus, S., Preibisch, T., & Ohnaka, K. 2008, *ApJ*, 676, 490
- Kraus, S., Hofmann, K.-H., Menten, K. M., Schertl, D., Weigelt, G., Wyrowski, F., Meil-land, A., Perraut, K., Petrov, R., Robbe-Dubois, S., Schilke, P., Testi, L. 2010, *Nature* 466, 339
- Krumholz, M. R., Klein, R. I., McKee, C. F., Offner, S. S. R., & Cunningham, A. J. 2009, *Science*, 323, 754
- Lada C.J., *IAUS*, 115, 1
- Mannings, V., & Sargent, A. I. 1997, *ApJ*, 490, 792
- Millan-Gabet, R., Malbet, F., Akeson, R., Leinert, C., Monnier, J., & Waters, R. 2007, *Protostars and Planets V*, 539
- Miroshnichenko, A., Ivezić, Ž., Vinković, D., & Elitzur, M. 1999, *ApJ*, 520, L115
- Robitaille, T. P., Whitney, B. A., Indebetouw, R., Wood, K. 2007, *ApJS* 169, 328
- Rowan-Robinson M. 1980, *ApJ* 44, 403
- Shu, F., Najita, J., Ostriker, E., Wilkin, F., Ruden, S., Lizano, S. 1994, *ApJ* 429, 781
- Waters, L. B. F. M., & Waelkens, C. 1998, *ARA&A*, 36, 233
- Weigelt, G., Grinin, V. P., Groh, J. H., Hofmann, K.-H., Kraus, S., Miroshnichenko, A. S., Schertl, D., Tambovtseva, L. V., Benisty, M., Driebe, T., Lagarde, S., Malbet, F., Meilland, A., Petrov, R., & Tatulli, E. 2011, *A&A*, 527, A103
- Whitney, B. A., Wood, K., Bjorkman, J. E., Wolff, M. J. 2003 *ApJ* 591, 1049
- Zhan Y. & Tan, J.C. 2011, *ApJ* 733, 55